ARTICLE IN PRESS

Life Sciences in Space Research xxx (xxxx) xxx

Contents lists available at ScienceDirect

Life Sciences in Space Research

journal homepage: www.elsevier.com/locate/lssr

Active radiation measurements over one solar cycle with two DOSTEL instruments in the Columbus laboratory of the International Space Station

Daniel Matthiä [a,*], Sönke Burmeister [b], Bartos Przybyla [a], Thomas Berger [a]

[a] German Aerospace Center (DLR), Institute of Aerospace Medicine, Cologne, Germany
[b] Christian Albrechts Universität zu Kiel (CAU), Kiel, Germany

ARTICLE INFO

Keywords:
International Space Station
South Atlantic anomaly
Galactic cosmic radiation
Absorbed dose
Dose equivalent
Exploration

ABSTRACT

Two DOSimetry TELescopes (DOSTELs) have been measuring the radiation environment in the Columbus module of the International Space Station (ISS) since 2009 in the frame of the DOSIS and DOSIS 3D projects. Both instruments have measured the charged particle flux rate and dose rates in a telescope geometry of two planar silicon detectors. The radiation environment in the ISS orbit is mostly composed by galactic cosmic radiation (GCR) and its secondary radiation and protons from the inner radiation belt in the South Atlantic Anomaly (SAA) with sporadic contributions of solar energetic particles at high latitudes. The data presented in this work cover two solar activity minima and corresponding GCR intensity maxima in 2009 and 2020 and the solar activity maximum and corresponding GCR intensity minimum in 2014/2015. Average dose rates measured in the Columbus laboratory in the ISS orbit from GCR and SAA are presented separately. The data is analyzed with respect to the effective magnetic shielding and grouped into different cut-off rigidity intervals. Using only measurements in magnetically unshielded regions at low cut-off rigidity and applying a factor for the geometrical shielding of the Earth, absorbed dose rates and dose equivalent rates in near-Earth interplanetary space are estimated for the years 2009 to 2022.

1. Introduction

Radiation exposure in Low-Earth-Orbit (LEO) is dominated by contributions from galactic cosmic radiation (GCR) and charged particles trapped in the Earth's radiation belts. GCR consists mostly of fully ionized atomic nuclei reaching Earth from interstellar space after propagating through the interplanetary medium. During their travel through the heliosphere, the intensity of GCR is modulated by the magnetic field carried by the solar wind, which leads to the variation in GCR intensity being anti-correlated to the solar activity. GCR nuclei from hydrogen to iron with energies between about 100 MeV/n and a few hundred GeV/n are considered relevant for the radiation exposure in space. The outer radiation belt contains mostly electrons with energies below a few MeV which do not affect dose rates inside the International Space Station (ISS) as they are effectively shielded by the outer walls of the modules and equipment installed and stored inside the ISS. The inner radiation belt, that the ISS crosses in the so-called South Atlantic Anomaly (SAA), on the other hand, also contains protons with energies up to several hundred MeV, that can penetrate the station walls and contribute to the exposure inside the station directly and through the secondary radiation field that is created by interactions with the station walls and equipment inside the station. Radiation exposure in LEO differs from exposure in near-Earth interplanetary space not only by the additional contributions from the radiation belts but is also affected by two major protective mechanism provided by the magnetic field of the Earth and the geometrical shielding from the body of the Earth, which covers a large fraction of the sky at LEO altitudes. Nevertheless, the comprehensive set of data that has been recorded within numerous projects onboard the ISS can be used not only to assess the exposure in the ISS but also to derive the radiation level that is to be expected in interplanetary space for spacecraft shielding conditions that are identical or very similar to the conditions for which the data in LEO were taken. Such data is important to estimate the exposure to be encountered on interplanetary missions and to validate models that by themselves can then be used for mission planning. Narici et al. (2015) have given an overview over measurements with so-called active radiation detectors performed onboard the ISS before 2015, for instance in the USLab, e.g. (Lee et al., 2007), Zvezda, e.g. (Labrenz et al., 2015; Lishnevskii et al., 2012; Petrov et al., 2006), and other locations in the ISS, e.g. (Semkova et al., 2010, 2014; Zábori and Hirn, 2012). The advantage of active

* Corresponding author.
E-mail address: daniel.matthiae@dlr.de (D. Matthiä).

https://doi.org/10.1016/j.lssr.2023.04.002
Received 19 January 2023; Received in revised form 31 March 2023; Accepted 6 April 2023
Available online 12 April 2023

radiation measurements is that they provide time resolved data in contrast to passive radiation measurements, that typically provide integrated dose values. The time resolved data allows to identify the different components of the radiation field, which can then be analyzed separately. To characterize the radiation field, dose rate measurements are accompanied by measurements that allow to quantify the biological impact of the radiation. Most often, this is done using the quality factor Q (ICRP, 1991, 2013), which is defined as a function of the unrestricted linear energy in water. In the DOSIS and DOSIS 3D (Berger et al., 2016, 2017) projects the exposure in terms of dose rates and quality factor has been measured in the Columbus laboratory of the ISS since 2009 with passive and active radiation detectors. The data recorded within the DOSIS and DOSIS 3D projects cover now more than one solar cycle and the projects have provided dose rate measurements of GCR and of particles from the inner radiation belt during crossings of the SAA by the ISS. In this publication we present data from the DOSimetry TELescopes (DOSTELs) instruments that have been measuring since the beginning of the DOSIS project in 2009. Procedures to identify the contribution from radiation belt particles in the SAA and the impact of the shielding effect of the Earth's magnetosphere and the shielding effect from the solid Earth are presented and the resulting estimate of the exposure in interplanetary space from GCR is given.

2. The DOSimetry TELescope DOSTEL

2.1. Instrument description

Each DOSTEL instrument consists of two circular silicon detectors (passivated implanted planar silicon, PIPS) with 14.85 mm radius (6.93 cm^2 area) and 315 μm thickness. The silicon detectors are arranged in a telescope geometry at a distance of 15 mm which allows to limit the maximum incident angle of measured particles to below approximately 60° against the normal of the detector plane, if the two detectors are used in coincident mode, i.e. if only events are considered which produce a signal in both planes. In coincidence mode the one-sided geometrical factor is 824 mm^2sr. Using the coincidence mode, the linear energy transfer (*LET*) spectra of the measured particles can be estimated using the energy deposition in a detector plane divided by the mean path length in the detector. For an assumed isotropic field the mean path length in the silicon detectors is 380 μm. The *LET* spectra measured in the detector can be used to calculate the quality factor Q of the radiation field, which is defined as a function of *LET* (ICRP, 1991). Energy deposition spectra are integrated over 45 min, i.e. approximately one half-orbit. The dose rate in silicon is measured by the sum of all energy depositions in a single detector plane divided by its mass and the measurement interval, which is either 20 s during crossings of the SAA or 100 s outside of the SAA; the switch between the measuring intervals is triggered by an algorithm using the change in measured count rate.

More detailed descriptions of the measurement setup containing data readout and data transfer can be found in Berger et al. (2016) and Berger et al. (2017).

2.2. DOSTEL on ISS

The DOSTEL instrument family has a long history for measuring the dose in space and had already been applied on various shuttle missions (Beaujean et al., 1999, 1999; Reitz et al., 1998; Singleterry et al., 2001) and on-board the space station MIR (Badhwar et al., 2002; Beaujean et al., 2002; Burmeister et al., 2000) before DOSTEL instruments were installed for dose measurements for the first time on the ISS in 2001 (Reitz et al., 2005) in the frame of the DosMap project. Further on, instruments of the DOSTEL family have been applied in paralled to DOSIS and DOSIS 3D in the frame of the MATROSHKA project (Labrenz et al., 2015). The measurements inside the Columbus laboratory of the ISS started in the frame of the DOSIS project in 2009 (Berger et al., 2016). With the start of DOSIS the two DOSTEL instruments were delivered together with the DOSTEL Data and Power Unit (DDPU) mounted within a NOMEX© pouch (DOSIS-MAIN-BOX) to the ISS and mounted at a fixed position beneath the European Physiology Module (EPM) in Columbus. The two DOSTEL instruments have been mounted perpendicular to each other; the viewing direction of the telescope is along the ISS flight direction for DOSTEL-1 (X) and perpendicular to the ISS flight direction for DOSTEL-2 (Y).

In addition to the active instruments also passive detector packages (PDPs) were delivered to monitor the radiation environment in Columbus at eleven fixed locations. Fig. 1 provides a picture of the EPM rack within the Columbus laboratory of the ISS showing in the orange frame one of the eleven PDPs mounted on top of EPM and in the blue frame beneath the EPM rack the DOSIS-MAIN-BOX. The relevant data cable connector for data transfer of the DOSTEL data via EPM to ground is shown in green.

During the time the DOSTEL instruments have been measuring it was possible at one hand to study the radiation environment in Columbus and to compare the data with other instruments on-board the ISS, for example the ALTEA instrument (Narici et al., 2017). Additionally, one of the two Ground Level Enhancements (GLEs) of solar cycle 24 could be measured in September 2017 and the corresponding dose caused by the solar energetic particles on ISS and measured by DOSTEL was compared with ISS-RAD data (Berger et al., 2018).

Further long-time analysis and comparison for the contribution of GCR was performed including data from MSL-RAD at the surface of Mars

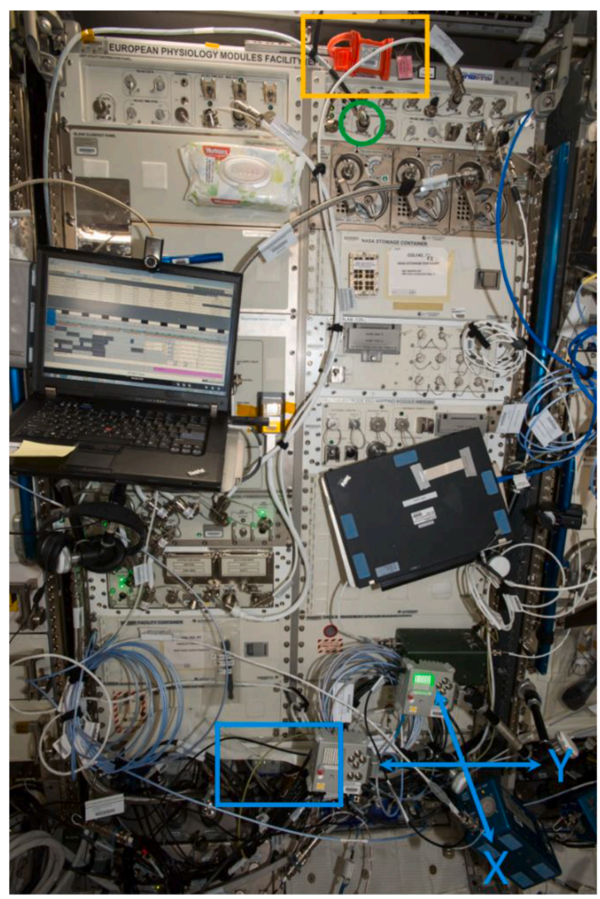

Fig. 1. The EPM rack in the European Columbus laboratory. The location of the DOSIS-MAIN-BOX with the two DOSTEL instruments is indicated by the blue box. The viewing directions of DOSTEL-1 (X, along ISS flight direction) and DOSTEL-2 (Y, perpendicular to ISS flight direction) are indicated by the arrows. The location of one of the PDPs mounted on top of EPM is highlighted by the orange box. The green circle indicates the data cable connected to the EPM rack for DOSTEL data downlink.

and CRaTER in lunar orbit and is given in Berger et al. (2020). This analysis comprised DOSTEL data until July 2019. In this work, additional data until December 2022 is provided covering the whole solar activity minimum between solar cycle 24 and 25 and the drop in GCR intensity in 2022.

3. Results

3.1. Dose rates in the ISS orbit

An important point of the DOSIS and the DOSIS 3D experiments has been that both the active DOSTEL instruments and the passive radiation detectors have been installed at the same locations since the beginning of the measurements. Accordingly, these detectors provide long term measurements of the radiation environment under relatively stable shielding conditions covering now more than one solar cycle. An overview of the data coverage of the DOSTEL-1 and the DOSTEL-2 instrument is provided in Table 1; in this work data until 20 December 2022 is used.

The DOSTEL instruments measure absorbed dose in the 6.93 cm^2 silicon detectors of the two instruments along the trajectory of the ISS. Fig. 2 shows dose rates measured by the DOSTEL-2 instrument averaged over three-month periods during solar maximum conditions (2014-01-01 – 2014-03-31, Fig. 2 top) and solar minimum conditions (2020-04-01 – 2020-06-30, Fig. 2 bottom) over the whole latitude range covered by the ISS orbit and the SAA region as a cut-out. The region of the SAA, covering large parts of South America and the South Atlantic, is clearly visible with dose rates exceeding the values outside this region by far. Dose rates in the center of the SAA reach values of about 10–20 mGy/d compared to maximum values of about 0.2 mGy/d at high latitudes during solar maximum and about 0.3 mGy/d during solar minimum. While differences in the dose rate in the SAA between solar minimum and maximum can partly be attributed to changes in the altitude of the ISS, the variation in the dose rate outside the SAA region is almost exclusively caused by the variation in the primary GCR intensity. The data shown in the figure also reflect the impact of the geomagnetic shielding, showing that the highest values at low geomagnetic shielding corresponding to regions of low cut-off rigidities at high latitudes and eastern longitudes in the southern hemisphere and western longitudes in the northern hemisphere, respectively.

Fig. 3 compares the measured total dose rate since 2009 with major factors impacting the exposure on the ISS: Fig. 3a provides the monthly and averaged Sun Spot Number (Sn; from: https://sidc.be/silso) as a marker for the solar activity and Fig. 3b shows the corresponding Oulu neutron monitor count rates (from: https://cosmicrays.oulu.fi/) as a marker for the cosmic ray intensity as measured on ground; cosmic ray intensity is anti-correlated to solar activity. The ISS altitude (Fig. 3c) has a large impact on the dose rate contributed by charged particles in the inner radiation belt, that the ISS crosses in the SAA region. These variations in the dose rate are caused by changes in the intensity of radiation belt particles when the ISS is moved deeper into the radiation belt at higher altitudes or towards the belt's boundaries for lower altitudes. The GCR dose rate, on the other hand, is mostly unaffected by altitude changes. The remaining atmosphere at ISS altitudes is negligible and does not provide any effective shielding from GCR. The small changes in magnetic and geometric shielding related to altitude changes of a few tens of km have no significant impact on the measured dose rate. The temporal variation of dose rates in silicon averaged over one day measured by DOSTEL-1 and DOSTEL-2 from 2009 to 2022 is illustrated in Fig. 3d. The measured dose rate contains contributions from GCR, SAA and several solar energetic particle events, the latter not being distinguishable from other variations, and roughly follows the changes in the cosmic ray intensity measured by Oulu with the exception of an observed increase of the measured dose rate in Columbus between 2011 and 2012. The relatively large change in altitude from about 340 km to 400 km in 2011 is the cause for the increased dose rates measured by the DOSTEL instruments. Without this effect, it could have been expected that the otherwise decreased cosmic ray intensity (Fig. 3b) would have led to a corresponding decrease of dose rate in Columbus. The higher altitude increased both the duration of the crossings of the radiation belt in the SAA and the particle fluxes and correspondingly the dose rates within the SAA. The decrease in altitude at the end of 2014 and the beginning of 2015 is also partly responsible for the decrease in the measured total dose rate at the time, but it also coincides with a decrease of cosmic ray intensity. The altitude of the ISS mainly affects the contribution of the SAA to the absorbed dose, and the total dose additionally varies within the solar cycle. The measurements with the DOSTEL units started in mid-2009 during a period of exceptionally low solar activity, which led to record high GCR intensities (Mewaldt et al., 2010) not measured since the beginning of the systematic measurement of GCR with neutron monitor stations in the 1950s and 1960s, let alone during the era of human space flight. Apart from an interruption between the DOSIS and DOSIS 3D projects in late 2011 and early 2012, the measurements covered the time of increasing solar activity and decreasing GCR intensity until the solar maximum was reached in 2014 – 2015 and the following decrease in solar activity and increase in GCR intensity towards the recent solar minimum in 2020. Recently, in 2022, the sun has entered a phase of increasing activity towards the next solar maximum of solar cycle 25. While much of the increase in dose rate measured between 2011 and 2012 can be attributed to the altitude change, most of the increase observed between 2015 (~0.15 mGy/day) and 2021 (0.3 mGy/day – 0.35 mGy/day) is caused by variations in the primary particle populations of GCR and radiation belt particles during the solar cycle.

3.2. Galactic cosmic radiation and radiation belts

The three major sources for the radiation measured in the ISS orbit are GCR, radiation belt particles and solar energetic particles. The sporadic occurrence of solar energetic particle events only rarely affects the exposure on the ISS during the largest events and only at high latitudes and low magnetic shielding. Normally these events do not contribute substantially to the integral mission exposure of astronauts. Most events are too weak to be measured inside the Columbus module by the DOSTEL detectors. Table 2 lists time intervals that were excluded in the further analysis of the exposure from GCR and the SAA due to the occurrence of strong solar energetic particle events, that were distinguishable in the DOSTEL data. For additional information about these events the reader is referred to Berger et al. (2018) and Berger et al. (2020). Event #1 was identified for the first time in the DOSTEL data during the in-depth analysis of the data for this evaluation.

In order to analyze the remaining contributors to the radiation exposure, the GCR and the radiation belt particles, in detail, the two components need to be separated. A method to separate the contributions from the inner radiation belt in the SAA to the dose rates measured by the DOSTEL instruments was described in (Berger et al., 2020). In this method, statistically highly significant increases of the dose rate at any given point above the expected dose rate from GCR based on

Table 1
Days of measurements for the DOSTEL-1 and DOSTEL-2 instruments in the frame of DOSIS and DOSIS 3D until 20 December 2022.

	DOSIS (2009 – 2011)	DOSIS 3D (2012 – 2022)	DOSIS+ DOSIS 3D
DOSTEL-1 (days)	290	2977	3267
DOSTEL-2 (days)	644	3438	4082

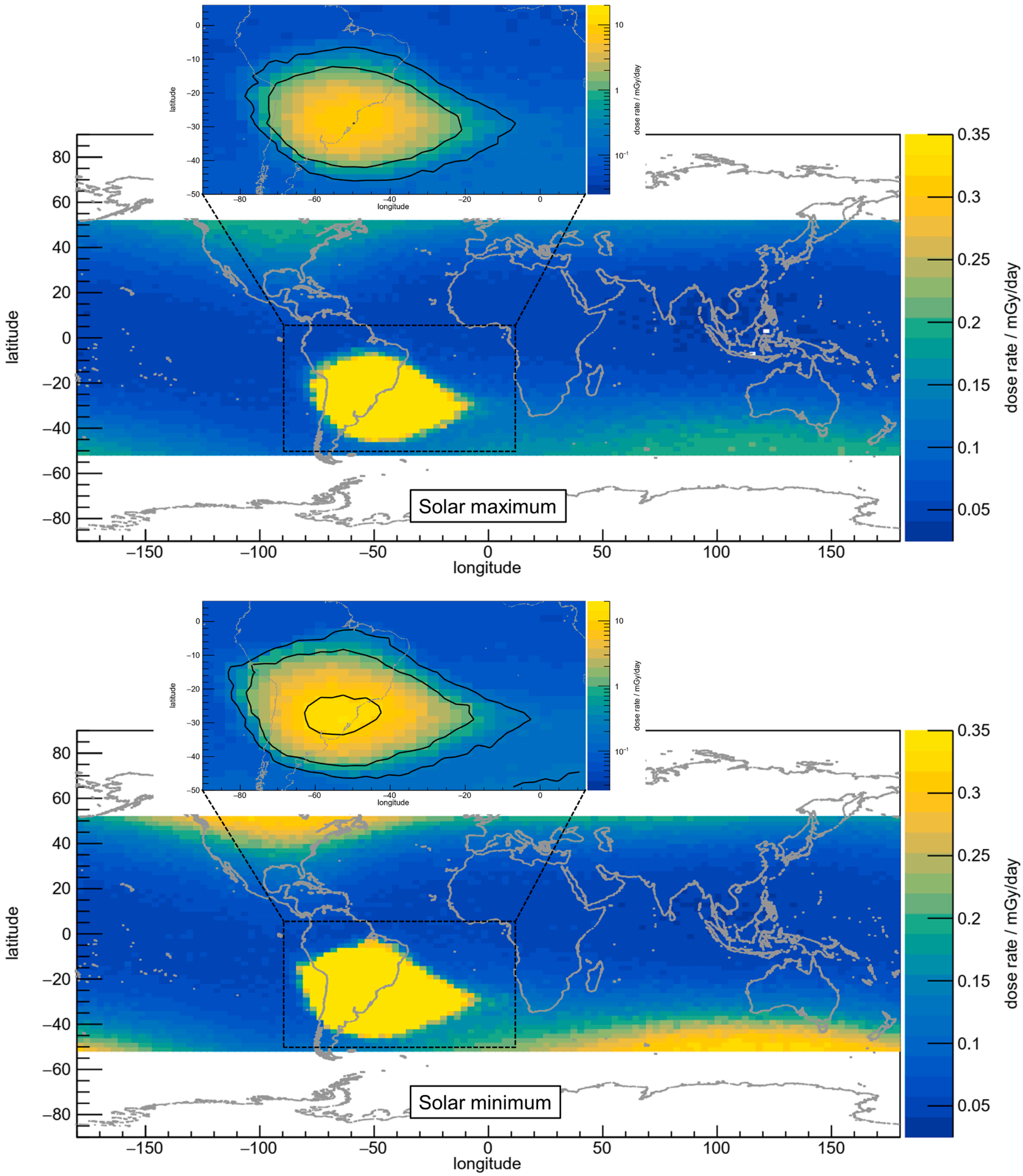

Fig. 2. Dose rate in silicon measured by DOSTEL-2 in ISS Orbit for solar maximum (top) and solar minimum (bottom) conditions. Cut-out regions show the area of the South Atlantic Anomaly (SAA) where dose rates are strongly increased due to charged particles from the inner radiation belt. Variations outside the SAA are caused by the geomagnetic shielding, that can be quantified by the cut-off rigidity (c.f. Section 3.2 and Fig. 6a). The contour lines in the SAA figures show thresholds to 0.2 mGy/d, 1 mGy/d and 10 mGy/d.

geomagnetic shielding are used to identify the region of the SAA. Based on this method, monthly averages from 2009 to 2022 of the dose rates from GCR and radiation belt particles in the SAA were calculated from the DOSTEL-1 and DOSTEL-2 measurements (Fig. 4a); the dose rates measured in the silicon detectors have been converted to dose in water using a factor of 1.23 in accordance with previous publications (Beaujean et al., 2002; Berger et al., 2017, 2020). From the separation of dose rates it becomes clear that most of the variations, that were observed in the total dose rate in Fig. 3d can be attributed to variations in the radiation belt. The intensity of the particle flux in the inner radiation belt varies during the solar cycle due to variations in the source process, i.e. the cosmic ray albedo neutron decay (CRAND), and the enhanced loss processes during solar active periods. While the average daily dose rate from SAA particles almost doubled between 2015 (DOSTEL-1: 0.08 mGy/day, DOSTEL-2: 0.10 mGy/d) and 2020 (DOSTEL-1: 0.20 mGy/day, DOSTEL-2: 0.25 mGy/d), the variation in the dose rate from GCR is only about 20%: from approximately 0.12 mGy/day during solar maximum to approximately 0.15 mGy/day during solar minimum. Fig. 4 also shows that the differences between DOSTEL-1 and DOSTEL-2 dose rate measurements can be almost exclusively attributed to differences in

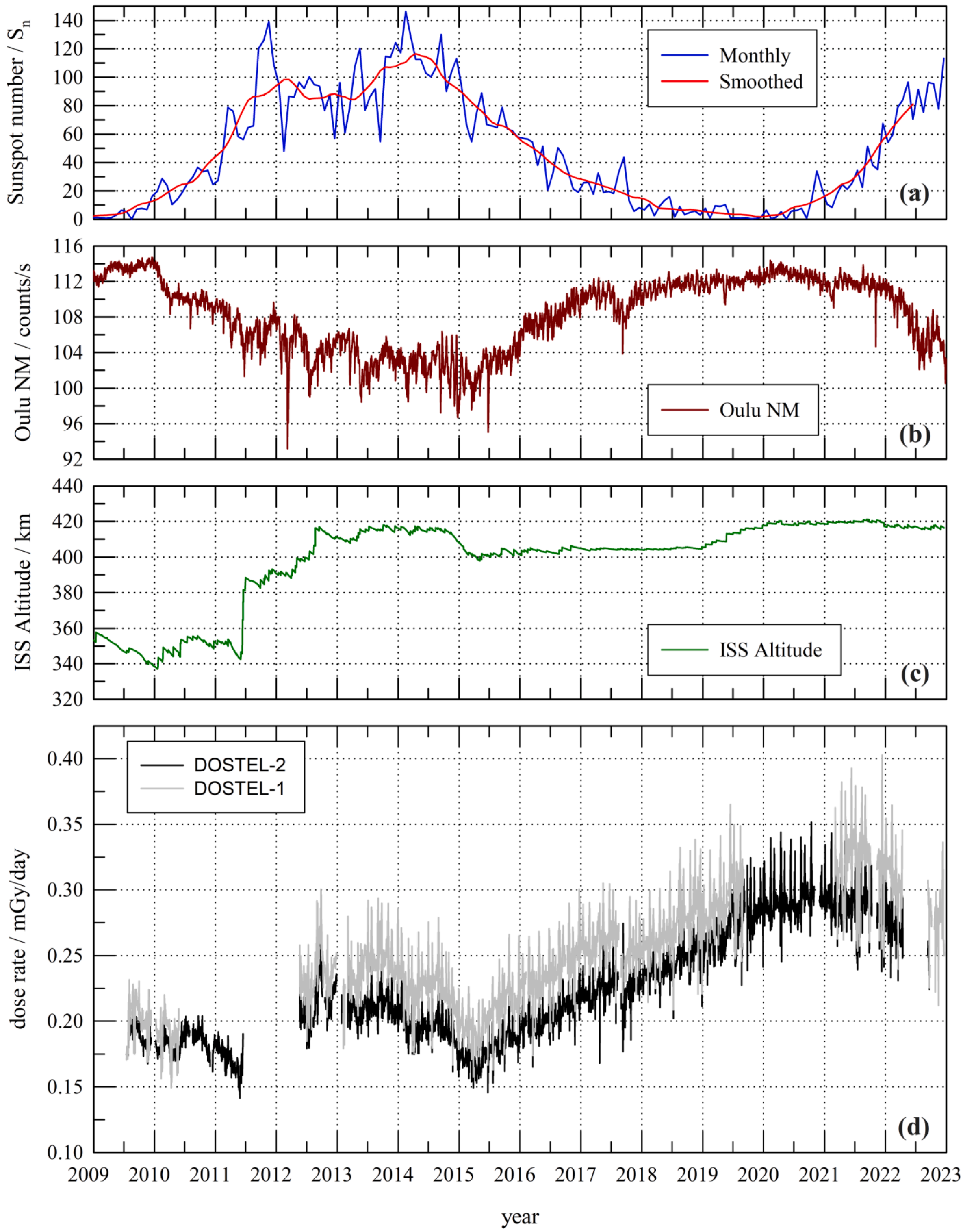

Fig. 3. (a) The monthly and 13 months smoothed sun spot number (Sn); (b) the Oulu neutron monitor counts rates; (c) the average ISS altitude; (d) the daily dose values as measured with the DOSTEL-1 and the DOSTEL-2 instruments in the frame of the DOSIS and DOSIS 3D project on board the Columbus laboratory of the ISS.

the measurements of the radiation belt particles. While dose rates from GCR measured by DOSTEL-1 and DOSTEL-2 agree within a few percent, the differences for the monthly averages of the dose rates in the SAA were between 10% and 40%, the latter occurring during solar maximum. The larger differences between the dose rate measurements in the SAA are caused by a combination of the orientations of DOSTEL-1 and DOSTEL-2 and the respective local shielding environment, which has a higher impact on the SAA particles.

In addition to the absorbed dose rate in Fig. 4a, Fig. 4b shows the rate of daily dose equivalent based on the measurement of the quality factor for the GCR and the SAA contributions. The quality factors are based on the average *LET* spectra over the whole project duration of DOSIS and DOSIS 3D measured by DOSTEL-1 for the relevant GCR and by DOSTEL-1 and DOSTEL-2 for the SAA crossings. For GCR a mean quality factor of $Q = 3.19 \pm 0.12$ was calculated and for the SAA $Q = 1.24 \pm 0.24$. The statistical uncertainties of the measurement of the quality factor are

Table 2
Time periods (UTC) with contributions from solar energetic particle events that have been excluded for the study of the dose from GCR.

#	Start (UTC)	End (UTC)	Previously described
1	07.06.2011 06:00	09.06.2011 00:00	
2	22.05.2013 12:00	24.05.2013 00:00	Berger et al. (2020)
3	06.01.2014 00:00	09.01.2014 00:00	
4	25.02.2014 00:00	27.02.2014 00:00	
5	02.09.2014 00:00	05.09.2014 00:00	
6	10.09.2014 21:00	12.09.2014 00:00	Berger et al. (2018)
7	11.09.2017 00:00	13.09.2017 00:00	

below 1% and can be neglected. The uncertainty given here is estimated from the expected variations in different viewing directions of the telescope by comparing the measurement of DOSTEL-1 and DOSTEL-2. The resulting total dose equivalent rate ranges from 0.5 mSv/day during solar maximum conditions in 2015 to around 0.8 mSv/day for solar minimum conditions in 2021. GCR contribute between 0.4 mSv/day and 0.5 mSv/day to these values, and the rest originates in radiation belt particles in the SAA.

In order to investigate the impact of the geomagnetic shielding on the dose rates, the measurements can be parameterized by the effective vertical cut-off rigidity R_C, here referred to simply as cut-off rigidity. In this context, the cut-off rigidity is interpreted as the lower threshold below which charged particles cannot reach a specific point in the magnetosphere and above which particles have access to the point of

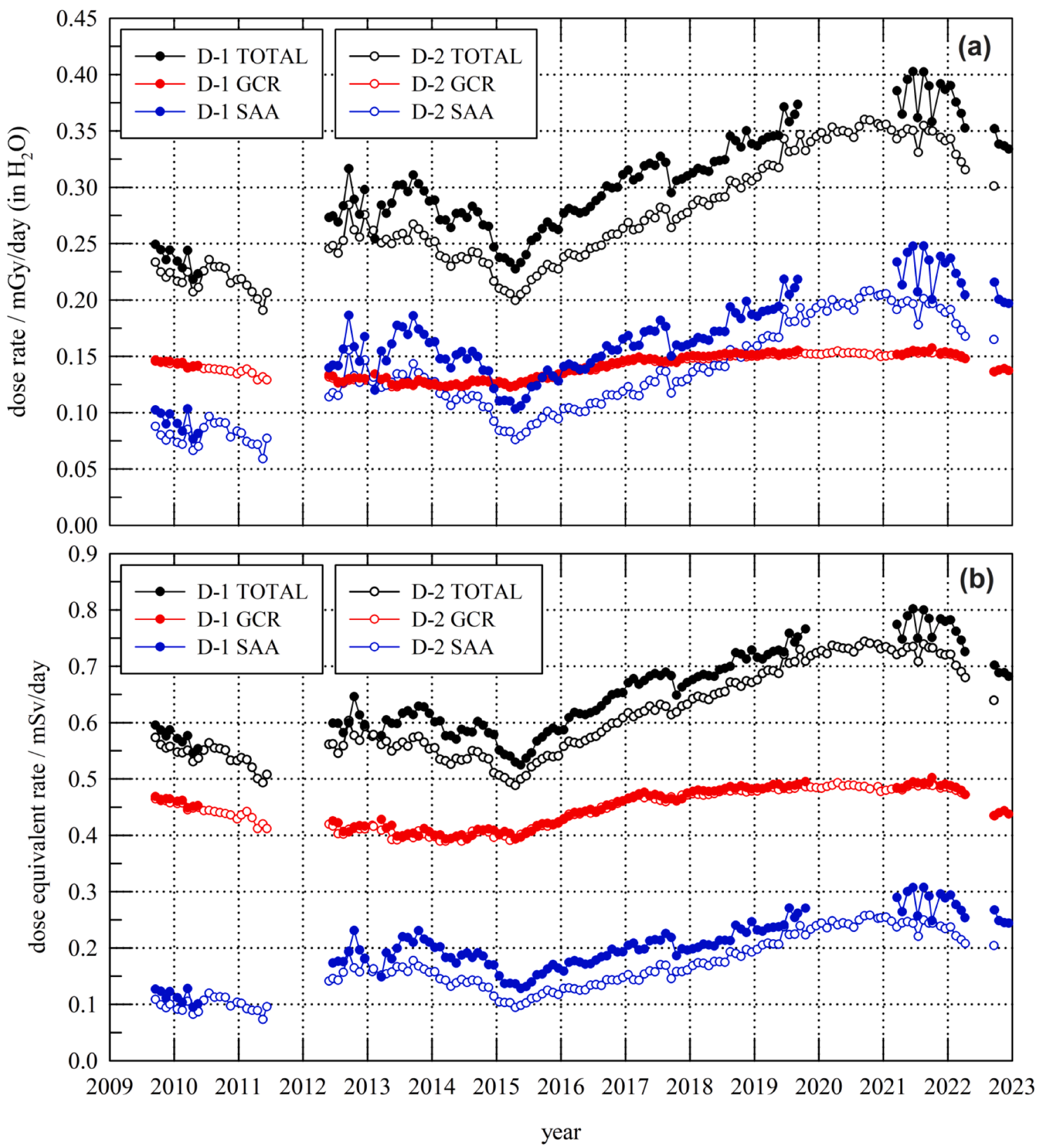

Fig. 4. (a) Total dose rates converted to dose in water and measured by DOSTEL-1 (D-1) and DOSTEL-2 (D-2) averaged over one-month intervals and the separation in contributions from GCR and SAA and (b) total dose equivalent rate calculated as product of the dose rate averaged over one month and the mean quality factor for GCR and SAA, respectively.

interest, for details see (Cooke et al., 1991; Shea et al., 1965). The lower the cut-off rigidity the weaker is the protection of the geomagnetic field against GCR. Towards high latitudes where the cut-off rigidity approaches zero, the shielding effect of the geomagnetic field is negligible. In general, the cut-off rigidity is a dynamic parameter that changes during geomagnetic disturbances and storms at time scales of hours and days and also slowly shifts with the variations of the internal magnetic field of Earth. Here, however, a static set of cut-off rigidities has been used that was calculated with PLANETOCOSMICS (http://cosray.unibe.ch/~laurent/planetocosmics) for the latest IGRF description of the internal field of Earth (Alken et al., 2021) for 1 January 2015 and the external field model by Tsyganenko (1989) at an altitude of 400 km. Variation in the internal field are expected to be small and are neglected in this work. Impacts of geomagnetic disturbances affect mostly regions of a few GV, where the cut-off rigidities can be significantly reduced during geomagnetic storms. Low cut-off rigidity regions that are the main focus for investigations concerning exploration are not affected by geomagnetic disturbances from space weather.

Fig. 5a illustrates the calculated cut-off rigidities reaching from 0 GV at high latitudes to about 16 GV close to the equator at around 100°E, where the maximum values are reached. Due to the tilt and shift of the dipole-like magnetic field of Earth against the rotational axis, the areas of low cut-off rigidity are not symmetrically distributed in the geographic coordinate system. The low cut-off rigidity region extends over a larger area on the southern hemisphere compared to the northern hemisphere. In its orbit at an inclination of 51.6° the ISS reaches cut-off rigidities $R_C < 0.5$ GV only at very limited regions at northern latitudes at around 80°W-100°W and at southern latitudes at approximately 80°E – 160°E. The ISS is located only about 2% of the time in regions with $R_C < 0.5$ GV. The effect of the magnetic shielding is obvious comparing the cut-off rigidity and the measured dose rates (Fig. 2) ignoring the contribution of the SAA.

Using the cut-off rigidities from Fig. 5a, the dose rate measurements can be parameterized according to the geomagnetic shielding. Fig. 5b and Fig. 5c contain the 27-day averages (one solar rotation) of the dose rate measured by DOSTEL-1 and DOSTEL-2 since 2009 versus the cut-off rigidity with SAA and solar energetic particle contributions removed. The figure illustrates the variation of the GCR dose rates over the solar cycle showing the largest variations at low cut-off rigidities. At high cut-off rigidities no variation can be recognized. This fact is investigated in the following section in more detail.

3.3. Relevance for exploration missions outside the magnetosphere

The protection by the geomagnetic field from GCR provided to the ISS LEO has been illustrated in the previous section. Additionally, the shadowing of the Earth reduces the number of primary GCR particles reaching the ISS. These two mechanisms are the main causes for differences in the dose rates from GCR at LEO compared to near-Earth interplanetary space, if identical or similar local shielding conditions by the spacecraft are assumed.

If the effect of geomagnetic shielding is investigated, it can be observed that the dose rates reach a maximum at small cut-off rigidities (Fig. 6a, errors bars show the standard deviation of the dose rates in each bin). Towards lower cut-off rigidities the absolute value of the derivative of the measured dose rate decreases and, depending on the solar activity and corresponding primary particle spectrum, the dose rate is approximately constant and forms a more or less pronounced plateau below about 0.7 GV (solar maximum) and 0.4 GV (solar minimum). The figure shows the dependency of the measured GCR dose rate on the geomagnetic shielding expressed by the cut-off rigidity for three different three-month periods representing solar minimum, intermediate and solar maximum conditions. For higher solar activity, which corresponds to a flatter spectrum at lower energies, the plateau extends to higher cut-off rigidities. For the purpose of estimating the dose rates outside the geomagnetic field measurements at locations of $R_C < 0.5$ GV can be considered as effectively unshielded. Fig. 6a also shows that magnetic shielding is more effective for low solar activity (highest GCR intensity; 2019-06-01 – 2019-09-01) compared to high solar activity (lowest GCR intensity; 2014-01-01 to 2014-04-01) because lower energetic particles contribute relatively less during solar active periods but are more affected by the geomagnetic field and the corresponding shielding effect.

The reduced variations during the solar cycle at higher geomagnetic shielding (greater cut-off rigidity) also show in Fig. 6b (errors bars show the standard deviation of the dose rates in each time interval), in which the time dependence of the measured dose rates at three different cut-off rigidity regions is illustrated: unshielded ($R_C < 0.5$ GV), intermediate (4 GV $\leq R_C < 5$ GV) and strong geomagnetic shielding ($R_C > 10$ GV). For strong geomagnetic shielding, the measured dose rate is approximately constant at around 0.05 mGy/d in silicon. In contrast, for no geomagnetic shielding, the dose rate increases by more than 50% from solar maximum conditions (≈0.2 mGy/d) to solar minimum conditions (≈0.32 mGy/d). Total dose rates in silicon and water for the three time intervals are given in Table 3 together with the dose equivalent rates for the identical time intervals using the average quality factor. The absorbed dose rate in Table 3 is given with the statistical uncertainties of the values which are below 1%; for the dose equivalent rate the systematical uncertainties of the quality factor is included.

The second effect reducing the intensity of cosmic radiation at low orbits is the obstruction by the Earth which decreases with increasing altitude. At an altitude of about 400 km the Earth blocks about 30% of the sky. The fraction of particles from interplanetary space measured at a corresponding orbit also depends on the angular distribution of the primary particles and the detector sensitivity. For GCR particles, which have an isotropic distribution, the fraction of particles reaching a certain altitude corresponds to the fraction that is not blocked by the Earth, i.e. approximately 70%. Approximating the Earth as a sphere, the corresponding shadow factor s at an altitude h_E can be calculated as

$$s = (1 - 0.5\cdot(1 - \cos(\arcsin(R_E / (R_E + h_E)))))$$

$R_E = 6371$ km is the mean radius of the Earth (https://nssdc.gsfc.nasa.gov/planetary/factsheet/earthfact.html). The inverse of the shadowing factor can be used to scale the measurements in orbit to obtain an estimate for the dose rates for which the effect of the shielding by the Earth is eliminated. If only measurements at values of $R_C < 0.5$ GV are used, one can obtain a good estimate for the corresponding value in interplanetary space. Fig. 7 shows 27-day averages of the altitude of the ISS (Fig. 7a) and the corresponding shadowing factor (Fig. 7b) for measurements in the region of $R_C < 0.5$ GV. As the data coverage was not identical for DOSTEL-1 and DOSTEL-2, the shadowing factor was individually calculated for each measuring point of the two detectors and averaged over 27 days. The impact of altitude variations of the ISS is small leading to shadowing factors between approximately 0.66 and 0.675. The inverse was used together with the 27-day averages of the dose rate at $R_C < 0.5$ GV (Fig. 6b) to calculate the expected dose rate in interplanetary space. Additionally, as above, a factor of 1.23 was applied to convert the measured dose rate in silicon to dose rate in water. Fig. 7c shows the resulting estimate of the dose rate in water in interplanetary space over the time interval of the DOSIS and DOSIS 3D experiments, i.e. between 2009 and 2022. The values extend from approximately 0.35 mGy/d during the solar maximum in 2014/2015 and 0.57 mGy/d and 0.58 mGy/d during the solar minima in 2009 and 2020, respectively.

With the average quality factor ($Q = 3.19 \pm 0.12$) from above, the dose rate in water can be converted to dose equivalent rate. The resulting estimate for the dose equivalent rate in free space derived from the DOSTEL-1 and DOSTEL-2 measurements and its variation is illustrated in Fig. 7c (grey markers, errors bars show the standard deviation of the dose rates in each time interval) with minimum values of about 1.1 mSv/d during solar maximum in 2014 and reaching peak values of about 1.9 mSv/d in 2009 and 2020. Again, the decrease of dose rates in 2022 related to the increasing solar activity of solar cycle 25 is clearly visible.

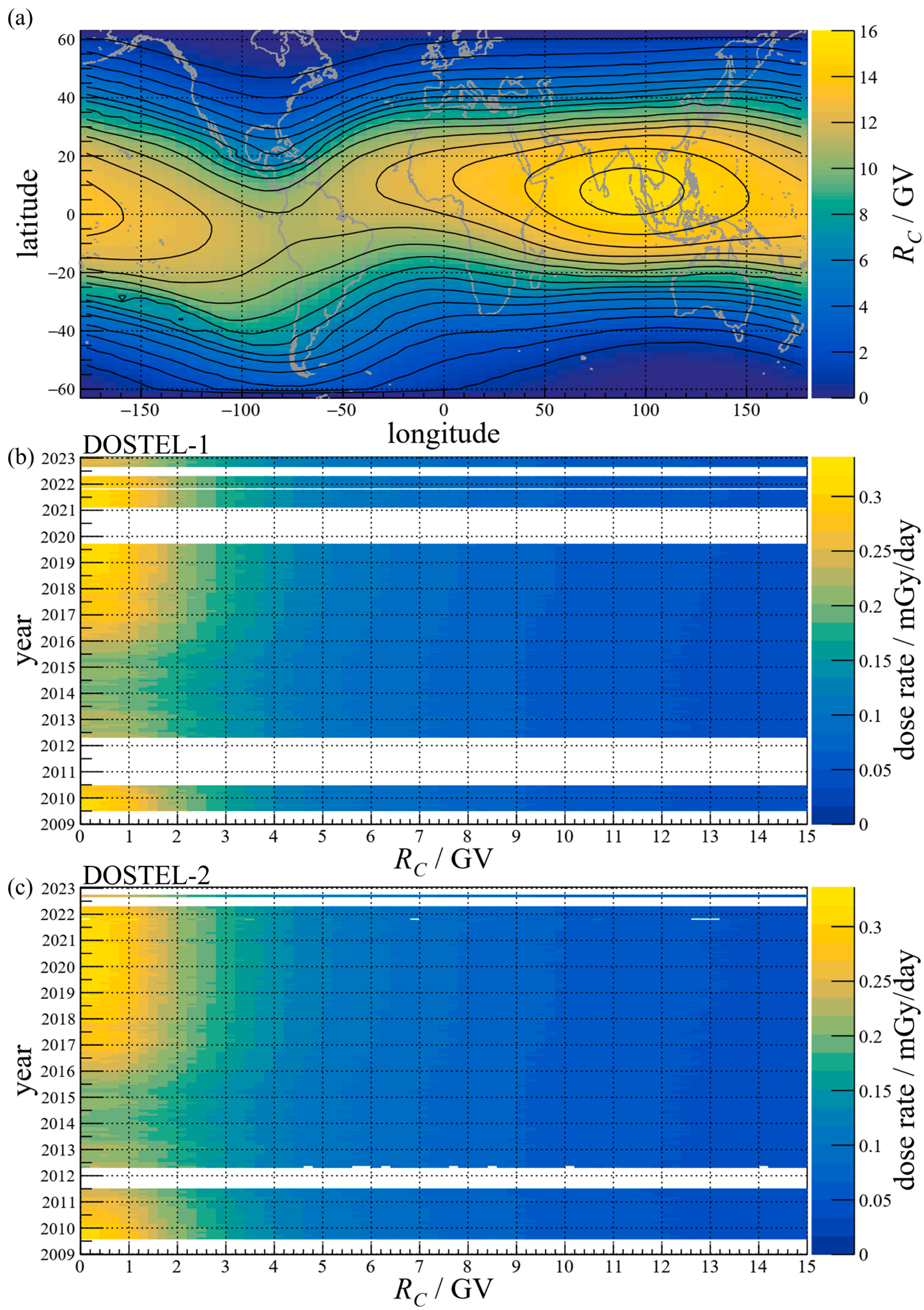

Fig. 5. (a) Effective vertical cut-off rigidity R_C calculated for an altitude of 400 km and temporal variation of the dose rate averaged over 27-day periods for GCR against effective cut-off rigidity measured by DOSTEL-1 (b) and DOSTEL-2 (c). Periods of energetic particle events as defined in Table 2 and SAA contributions were removed.

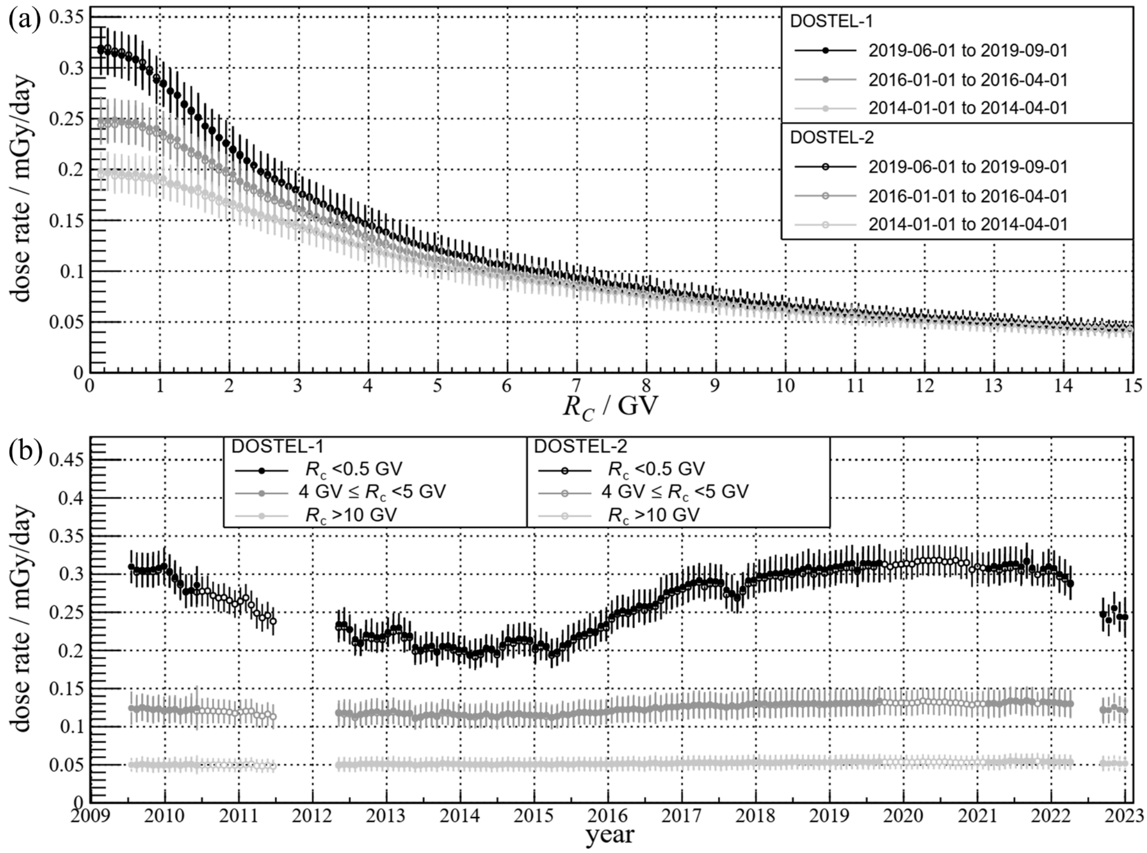

Fig. 6. (a) Dose rate in Si versus cut-off rigidity R_C measured by DOSTEL-1 and DOSTEL-2 and averaged over three month periods for solar minimum (2019), solar maximum (2014) and intermediate (2016) solar activity; b) GCR dose rate in Si measured by DOSTEL-1 and DOSTEL-2 averaged over one solar rotation (27 days) for different magnetic shielding intervals. Periods of energetic particle events as defined in Table 2 and SAA contributions were removed.

Table 3
Measured mean dose rate in silicon d_{Si} in three month intervals during solar minimum, solar maximum and intermediate solar activity and the derived dose rate in water d_{H2O} and dose equivalent rate h measured by DOSTEL-2 with uncertainties (unc.).

	ISS orbit averaged dose rates from GCR							
	d_{Si} mGy/day	unc.	d_{H2O} mGy/day	unc.	Q	unc.	h mSv/day	unc.
Solar minimum*	0.130	<1%	0.160	<1%	3.19	0.12	0.51	0.02
Intermediate*	0.114		0.141				0.45	0.02
Solar maximum*	0.103		0.126				0.40	0.02

* Solar minimum: 2020-04-01 – 2020-07-01; intermediate: 2016-01-01 – 2016-04-01; solar maximum: 2014-01-01 – 2014-04-01.

The values for three selected three-month intervals representing solar minimum, intermediate and solar maximum activity are given in Table 4. The calculation is based on the average dose rates in silicon measured by DOSTEL-2 in the respective intervals. Conversion to dose rate in water is again performed using the conversion factor of 1.23. Applying the average quality factor results in the mean dose equivalent rate at low cut-of rigidities, i.e. without relevant geomagnetic shielding. The values for low geomagnetic shielding are then divided by the corresponding shadow factor to obtain the estimates of the dose rates in near-Earth free space: 0.35 mGy/d and 1.13±0.04 mSv/d during solar maximum conditions and 0.58 mGy/d and 1.85±0.07 mSv/d during solar minimum conditions; uncertainties of the dose equivalent rate include the uncertainty of the quality factor. It has to be emphasized that these estimates are valid under the assumption, that the local mass shielding distribution is similar to the actual measurement environment, i.e. for a spacecraft with shielding similar to the Columbus module. Based on the shielding distribution used in Berger et al. (2018), derived with a ray-tracing technique from a CAD model of Columbus (Lee et al., 2016; Rios, 2018; Stoffle et al., 2012), the median shielding at the DOSTEL location is 36.9 g/cm^2. Also, a small contribution from albedo particles to the original measurements can be expected which would not be present in free space. This contribution, however, is expected to be small. Sato et al. (2011), for instance, estimated the combined contribution of albedo protons and neutrons to be approximately 4% of the effective dose equivalent and less than 1% for the skin dose equivalent. The quality factor applied to convert the absorbed dose to dose equivalent is expected to somewhat underestimate the quality factor in free space as it is based on measurements over the orbit of ISS. The quality factor at higher geomagnetic shielding is lower than at lower geomagnetic shielding as the average energy of the primary particles is higher. Higher energetic particles have, on average, a lower *LET* and a lower quality factor. This effect is most pronounced for heavy ions, but the relatively high mass shielding of Columbus leads to the fragmentation of the majority of the heavy ions. Accordingly, it can be assumed that this is a small effect for a shielding environment as Columbus. For a subset of DOSTEL data, Kollhoff (2015) has calculated that for the cut-off rigidity interval from 0 GV to 5 GV this effect increases the quality factor by approximately 3% against the orbit average.

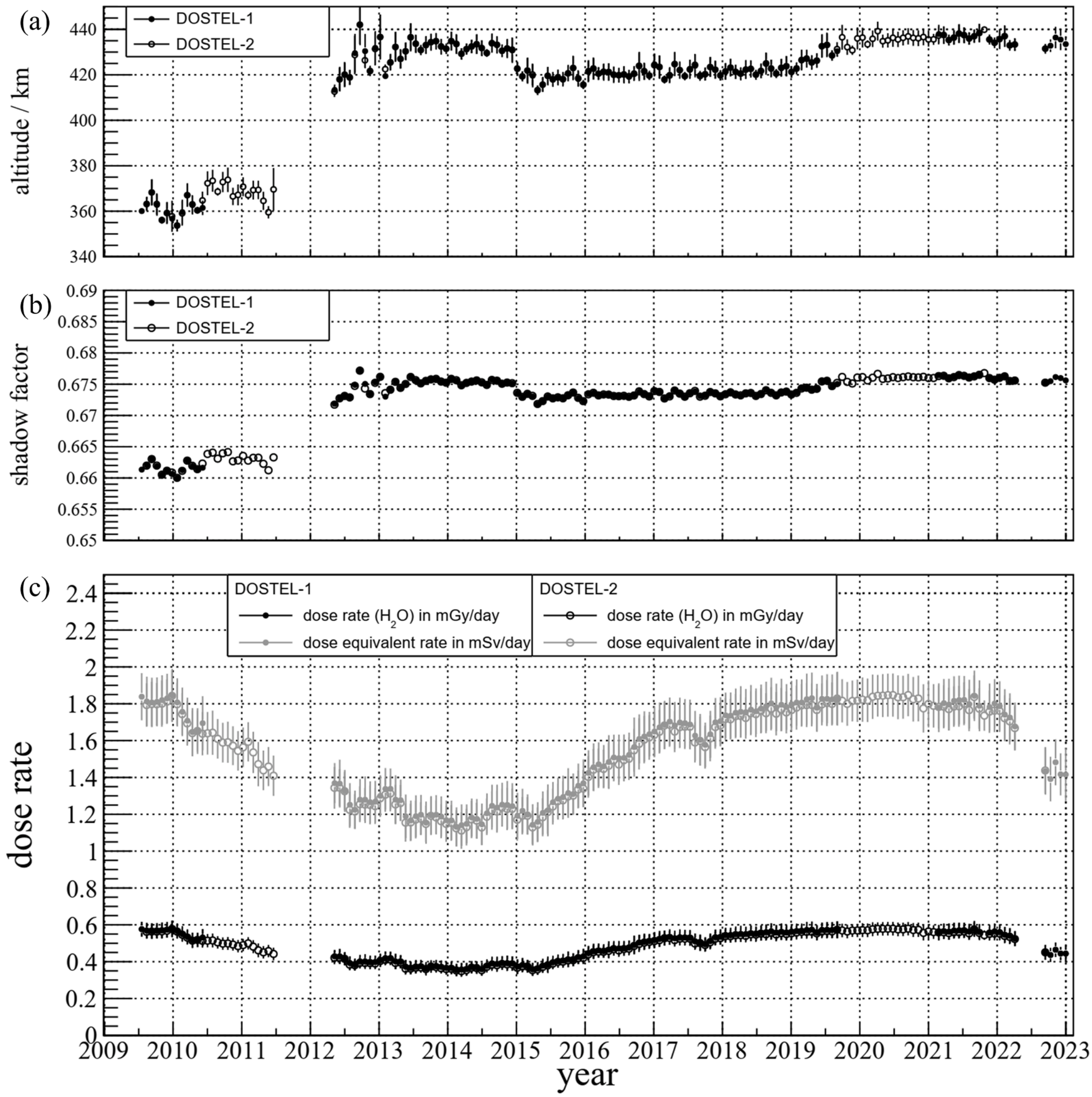

Fig. 7. 27-day averages of the altitude (a) and corresponding shadow factors (b) and the resulting estimated dose rate in water and dose equivalent rate in free space (c).

Table 4
Estimates of dose rates d and dose equivalent rates h in free space derived from measurements of DOSTEL-2 in low cut-off rigidity regions ($R_C < 0.5$ GV) and applying an altitude dependent correction factor (1/shadow factor) with uncertainties (unc.).

	Calculation of dose rates in free space based on data for $R_C < 0.5$ GV											
	$R_C < 0.5$ GV at ISS altitude								Free space estimate			
	d_{H2O} mGy/day	unc.	Q	unc.	h mSv/day	unc.	shadow factor	unc.	d_{H2O} mGy/day	unc.	h mGy/day	unc.
Solar minimum*	0.391	<1%	3.19	0.12	1.25	0.05	0.676	<1%	0.578	<1%	1.85	0.07
Intermediate*	0.301				0.96	0.04	0.673		0.447		1.43	0.05
Solar maximum*	0.239				0.76	0.04	0.675		0.354		1.13	0.04

* Solar minimum: 2020-04-01 – 2020-07-01; intermediate: 2016-01-01 – 2016-04-01; solar maximum: 2014-01-01 – 2014-04-01.

4. Summary

The two DOSTEL instruments have been measuring the radiation environment in the Columbus laboratory of the ISS for almost 13 years, starting in 2009. The data cover the solar cycle 24 and the initial phase of solar cycle 25 and peak GCR intensities in 2009 and 2020 and minimum intensities in the years 2014 and 2015 were measured. At altitudes of about 400 km – 420 km, which was the approximate altitude range after 2012, the total dose rate was between 0.16 mGy/day in silicon or 0.20 mGy/day in water during solar maximum conditions and about twice these values during solar minimum conditions. The contribution of radiation belt particles in the SAA was about 40% during solar maximum (2015) and about 60% during solar minimum (2020/2021). The higher SAA contribution in 2020/2021 is partly explained by an altitude increase in 2019, which lifted the ISS from 400 km to 420 km.

The mean quality factor measured between 2009 and 2022 was 3.19 $\pm$0.12 for GCR and 1.24$\pm$0.24 for contributions of radiation belt particles in the SAA. The resulting total dose equivalent rates were between 0.5 mSv/day in 2015 and up to 0.8 mSv/day in 2021.

The extreme values of the dose rates from GCR were reached in 2014 (GCR intensity minimum) and 2020 (GCR intensity maximum). The measured orbit-averaged dose rates from GCR in the Columbus laboratory at these times were 0.10 mGy/d in silicon, 0.13 mGy/d in water and 0.40$\pm$0.02 mSv/d during solar maximum in 2014 and 0.13 mGy/d in silicon, 0.16 mGy/d in water and 0.51$\pm$0.02 mSv/d in the solar minimum in 2020 (statistical uncertainties of dose rates are below 1%).

Considering the shielding effect of the Earth's magnetic field, effectively unshielded regions were selected by using low cut-off rigidity regions (<0.5 GV). The results were corrected for the shadowing effect of Earth in LEO to estimate the dose rates that would be expected in free space under similar mass shielding conditions. Estimates for the dose rates in water during solar minimum (2020) and maximum conditions (2014) are 0.58 mGy/d, 1.85$\pm$0.07 mSv/d and 0.35 mGy/d, 1.13$\pm$0.04 mSv/d, respectively. For the current NASA career dose limit of 600 mSv (NASA, 2022), this would correspond to a maximum mission duration of 314 days during solar minimum and 513 days during solar maximum. For the current ESA career limit of 1 Sv (ECSS, 2010; Straube et al., 2010), it would correspond to a maximum mission duration of 524 days during solar minimum and 855 days during solar maximum. It is important to note that the corresponding dose limits are for protection quantities that differ from the measured dose equivalent in the detector, namely NASA effective dose (NASA, 2013) and effective dose (ECSS, 2008). The relevant quantities are whole body quantities based on numerical phantoms using weighted sums of organ doses within the phantoms. Model calculations show that the measured dose equivalent is a conservative estimate of the corresponding protection quantities, which are typically 30% – 40% lower due to the additional self-shielding effect of the body. Accordingly, the estimates on the derived mission durations within the dose limits can be understood as lower limits.

Declaration of Competing Interest

The authors declare that they have no known competing financial interests or personal relationships that could have appeared to influence the work reported in this paper.

Acknowledgements

For DOSIS and DOSIS 3D DLR was supported by the DLR grant FuE-Projekt ''ISS LIFE'' (Programm RF-FuW, Teilprogramm 475). CAU, was supported by DLR under Grants 50WB0826, 50WB1026, 50WB1232 and 50WB1533. The authors gratefully acknowledge the support of ESA, especially the DOSIS 3D Project Integration Manager (PIM), Lukas DeSmet and Christopher Puhl. DOSTEL data downlink in the frame of DOSIS and DOSIS 3D was performed by colleagues from CADMOS, Toulouse, France. Further on we thank all our colleagues from DOSIS-OPS at DLR-MUSC, Germany. DOSIS 3D-DOSTEL data are available at: http://swe.ssa.esa.int/human-space-flight

The authors would like to thank the Sodankyla Geophysical Observatory and the website teams (http://cosmicrays.oulu.fi) for providing the Oulu neutron monitor data. The authors would like to thank the Royal Observatory of Belgium, Brussels for providing the sunspot data (http://www.sidc.be/silso/). The trajectory of ISS has been analyzed based on Two-line Element Set data provided by https://www.space-track.org/.

Finally, the authors greatly acknowledge all the help and support from our astronauts for DOSIS and DOSIS 3D.

References

Alken, P., Thébault, E., Beggan, C.D., Amit, H., Aubert, J., Baerenzung, J., et al., 2021. International geomagnetic reference field: the thirteenth generation. Earth, Planets Space 73 (1), 49. https://doi.org/10.1186/s40623-020-01288-x.

Badhwar, G.D., Atwell, W., Reitz, G., Beaujean, R., Heinrich, W., 2002. Radiation measurements on the Mir Orbital Station. Radiat. Meas. 35 (5), 393–422. https://doi.org/10.1016/S1350-4487(02)00072-0.

Beaujean, R., Kopp, J., Reitz, G., 1999a. Active dosimetry on recent space flights. Radiat. Prot. Dosimetry 85 (1–4), 223–226. https://doi.org/10.1093/oxfordjournals.rpd.a032839.

Beaujean, R., Reitz, G., Kopp, J., 1999b. Recent European measurements inside biorack. Mutation Res./Fundamental Mol. Mech. Mutagenesis 430 (2), 183–189. https://doi.org/10.1016/S0027-5107(99)00129-3.

Beaujean, R., Kopp, J., Burmeister, S., Petersen, F., Reitz, G., 2002. Dosimetry inside MIR station using a silicon detector telescope (DOSTEL). Radiat. Meas. 35 (5), 433–438. https://doi.org/10.1016/S1350-4487(02)00074-4.

Berger, T., Przybyla, B., Matthiä, D., Reitz, G., Burmeister, S., Labrenz, J., et al., 2016. DOSIS & DOSIS 3D: long-term dose monitoring onboard the Columbus Laboratory of the International Space Station (ISS). J. Space Weather Space Clim. 6 https://doi.org/10.1051/swsc/2016034.

Berger, T., Burmeister, S., Matthiä, D., Przybyla, B., Reitz, G., Bilski, P., et al., 2017. DOSIS & DOSIS 3D: radiation measurements with the DOSTEL instruments onboard the Columbus Laboratory of the ISS in the years 2009–2016. J. Space Weather Space Clim. 7, A8. https://doi.org/10.1051/swsc/2017005.

Berger, T., Matthiä, D., Burmeister, S., Lee, K., Rios, R.R., Semones, E., et al., 2018. The solar particle event from September 2017 as observed onboard the International Space Station (ISS). Space Weather 16, 1173–1189. https://doi.org/10.1029/2018SW001920.

Berger, T., Matthiä, D., Burmeister, S., Zeitlin, C., Rios, R., Stoffle, N., et al. (2020). Long term variations of galactic cosmic radiation on board the International Space Station, on the moon and on the surface of mars. 10, 34. 10.1051/swsc/2020028.

Burmeister, S., Beaujean, R., Kopp, J., Reitz, G., 2000. Data on radiation belt and solar energetic particles deduced from dosimetry in low earth orbits. In: Paper presented at the 5th Workshop on Radiation Monitoring for the International Space Station. Louvain-La-Neuve, Belgium. http://www.wrmiss.org/workshops/fifth/burmeister.pdf.

Cooke, D.J., Humble, J.E., Shea, M.A., Smart, D.F., Lund, N., Rasmussen, I.L., et al., 1991. On cosmic-ray cut-off terminology. Il Nuovo Cimento C 14 (3), 213–234. https://doi.org/10.1007/bf02509357 journal article.

ECSS. (2008). ECSS-E-ST-10-12C – methods for the calculation of radiation received and its effects, and a policy for design margins (15 November 2008) + "identified typographical error". Retrieved from https://ecss.nl/get_attachment.php?file=standards/ecss-e/ECSS-E-ST-10-12C15November2008.pdf.

ECSS. (2010). ECSS-E-HB-10-12A – calculation of radiation and its effects and margin policy handbook (17 December 2010). Retrieved from https://ecss.nl/get_attachment.php?file=handbooks/ecss-e-hb/ECSS-E-HB-10-12A17December2010.pdf.

ICRP, 1991. 1990 recommendations of the International Commission on Radiological Protection. Ann. ICRP 21 (1–3), 1–201.

ICRP, 2013. ICRP, 123. Assessment of radiation exposure of astronauts in space. ICRP Publication 123 Ann. ICRP 42 (4), 1–339. https://doi.org/10.1016/j.icrp.2013.05.004.

Kollhoff, A.L., 2015. Untersuchung Von LET Spektren der Galaktischen Kosmischen Strahlung in Abhängigkeit vom Erdmagnetfeld. Christian-Albrechts-Universitätzu Kiel (Bachelor).

Labrenz, J., Burmeister, S., Berger, T., Heber, B., Reitz, G., 2015. Matroshka DOSTEL measurements onboard the International Space Station (ISS). J. Space Weather Space Clim. 5, A38. https://doi.org/10.1051/swsc/2015039.

Lee, K., Flanders, J., Semones, E., Shelfer, T., Riman, F., 2007. Simultaneous observation of the radiation environment inside and outside the ISS. Adv. Space Re. 40 (11), 1558–1561. https://doi.org/10.1016/j.asr.2007.02.083.

Lee, K., Semones, E., Nounu, H.N., Stoffle, N., Barzilla, J., Gaza, R., Rios, R., 2016. Comparison of RAM dose data with calculated dose using an updated ISS CAD. In: Paper presented at the 21st Workshop on Radiation Monitoring for the International Space Station. Noordwijk, The Netherlands. http://www.wrmiss.org/workshops/twentyfirst/Lee.pdf.

Lishnevskii, A., Panasyuk, M., Benghin, V., Petrov, V., Volkov, A., Nechaev, O.Y., 2012. Variations of radiation environment on the International Space Station in 2005–2009. Cosmic Res. 50 (4), 319–323.

Mewaldt, R.A., Davis, A.J., Lave, K.A., Leske, R.A., Stone, E.C., Wiedenbeck, M.E., et al., 2010. Record-setting cosmic-ray intensities in 2009 and 2010. Astrophys. J. Lett. 723 (1), L1. https://doi.org/10.1088/2041-8205/723/1/L1.

Narici, L., Berger, T., Matthiae, D., Reitz, G., 2015. Radiation measurements performed with active detectors relevant for human space exploration. Front. Oncol. 5 https://doi.org/10.3389/fonc.2015.00273.

Narici, L., Berger, T., Burmeister, S., Di Fino, L., Rizzo, A., Matthiä, D., Reitz, G., 2017. Exploiting different active silicon detectors in the International Space Station: ALTEA and DOSTEL galactic cosmic radiation (GCR) measurements. J. Space Weather Space Clim. 7, A18. https://doi.org/10.1051/swsc/2017016.

NASA. (2013). Space radiation cancer risk projections and uncertainties –2012 (NASA-STD-3001, volume 1). Retrieved from https://spaceradiation.jsc.nasa.gov/irModels/TP-2013-217375.pdf.

NASA. (2022). NASA space flight human-system standard volume 1: crew health (NASA-STD-3001, volume 1, revision B). Retrieved from https://standards.nasa.gov/sites/default/files/standards/NASA/B//2022-01-05-NASA-STD-3001-Vol1-Rev-B-Final-Draft-Signature-010522.pdf.

Petrov, V.M., Bengin, V.V., Shurshakov, V.A., Panasyuk, M.I., Kutuzov, Y.V., Morozov, O. V., et al., 2006. Absorbed doses in October–November 2003 onboard the Russian segment of the International Space Station according to the data of radiation control system. Cosmic Res. 44 (2), 106–110. https://doi.org/10.1134/S0010952506020031.

Reitz, G., Beaujean, R., Heilmann, C., Kopp, J., Leicher, M., Strauch, K., 1998. Results of dosimetric measurements in space missions. Adv. Space Res. 22 (4), 495–500. https://doi.org/10.1016/S0273-1177(98)01069-2.

Reitz, G., Beaujean, R., Benton, E., Burmeister, S., Dachev, T., Deme, S., et al., 2005. Space radiation measurements on-board ISS—the DOSMAP experiment. Radiat. Prot. Dosimetry 116 (1–4), 374–379. https://doi.org/10.1093/rpd/nci262.

Rios, R., 2018. Timepix utilization on the International Space Station. In: Paper presented at the 23rd Workshop on Radiation Monitoring for the International Space Station. Tsuruga, Japan. https://wrmiss.org/workshops/twentythird/Zeitlin_S6.pdf.

Sato, T., Endo, A., Sihver, L., Niita, K., 2011. Dose estimation for astronauts using dose conversion coefficients calculated with the PHITS code and the ICRP/ICRU adult reference computational phantoms. Radiat. Environ. Biophys. 50 (1), 115–123. https://doi.org/10.1007/s00411-010-0330-0.

Semkova, J., Koleva, R., Maltchev, S., Kanchev, N., Benghin, V., Chernykh, I., et al., 2010. Radiation measurements inside a human phantom aboard the International Space Station using Liulin-5 charged particle telescope. Adv. Space Res. 45 (7), 858–865. https://doi.org/10.1016/j.asr.2009.08.027.

Semkova, J., Dachev, T., Koleva, R., Bankov, N., Maltchev, S., Benghin, V., et al., 2014. Observation of radiation environment in the International Space Station in 2012–March 2013 by Liulin-5 particle telescope. J. Space Weather Space Clim. 4, A32. https://doi.org/10.1051/swsc/2014029.

Shea, M.A., Smart, D.F., McCracken, K.G., 1965. A study of vertical cutoff rigidities using sixth degree simulations of the geomagnetic field. J. Geophys. Res. (1896-1977) 70 (17), 4117–4130. https://doi.org/10.1029/JZ070i017p04117.

Singleterry, R.C., Badavi, F.F., Shinn, J.L., Cucinotta, F.A., Badhwar, G.D., Clowdsley, M. S., et al., 2001. Estimation of neutron and other radiation exposure components in low earth orbit. Radiat. Meas. 33 (3), 355–360. https://doi.org/10.1016/S1350-4487(01)00049-X.

Stoffle, N., Welton, A., Barzilla, J., Gaza, R., Lee, K., Zapp, N., 2012. CAD shielding analysis of the International Space Station. In: Paper presented at the 17th Workshop on Radiation Monitoring for the International Space Station. Austin, Texas, USA. http://www.wrmiss.org/workshops/seventeenth/Stoffle.pdf.

Straube, U., Berger, T., Reitz, G., Facius, R., Fuglesang, C., Reiter, T., et al., 2010. Operational radiation protection for astronauts and cosmonauts and correlated activities of ESA medical operations. Acta Astronaut. 66 (7), 963–973. https://doi.org/10.1016/j.actaastro.2009.10.004.

Tsyganenko, N., 1989. A magnetospheric magnetic field model with a warped tail current sheet. Planet Space Sci. 37 (1), 5–20.

Zábori, B., Hirn, A., 2012. TriTel 3 dimensional space dosimetric telescope in the European Student Earth Orbiter project of ESA. Acta Astronaut. 71, 20–31. https://doi.org/10.1016/j.actaastro.2011.08.010.